NANO LETTERS

Letter

Deconvoluting Lipid Nanoparticle Structure for Messenger RNA Delivery

Yulia Eygeris, Siddharth Patel, Antony Jozic, and Gaurav Sahay*

Cite This: https://dx.doi.org/10.1021/acs.nanolett.0c01386

Read Online

ACCESS | Metrics & More | Article Recommendations | Supporting Information

ABSTRACT: Lipid nanoparticle (LNP) packaged mRNA vaccines have been deployed against infectious diseases such as COVID-19, yet their structural features remain unclear. Cholesterol, a major constituent within LNPs, contributes to their morphology that influences gene delivery. Herein, we examine the structure of LNPs containing cholesterol derivatives using electron microscopy, differential scanning calorimetry, and membrane fluidity assays. LNPs formulated with C24 alkyl derivatives of cholesterol show a polymorphic shape and various degrees of multilamellarity and lipid partitioning, likely due to phase separation. The addition of methyl and ethyl groups to the C24 alkyl tail of the cholesterol backbone induces multilamellarity (>50% increase compared to cholesterol), while the addition of a double bond induces lipid partitioning (>90% increase compared to cholesterol). LNPs with multilamellar and faceted structures, as well as a lamellar lipid phase, showed higher gene transfection. Unraveling the structure of mRNA-LNPs can enable their rational design toward enhanced gene delivery.

KEYWORDS: *mRNA delivery, lipid nanoparticles, cryo-TEM, gene therapy*
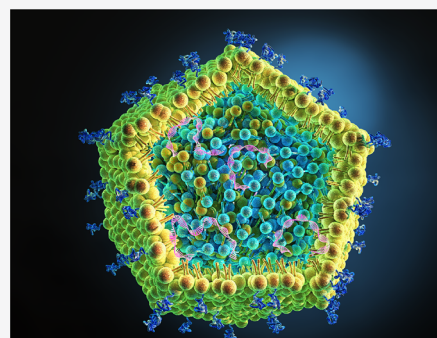
INTRODUCTION

mRNA-based therapies and vaccines hold tremendous potential for the treatment and prevention of a wide range of diseases, including cancer, genetic disorders, and infectious diseases.[1−4] For example, the first potential mRNA vaccine against SARS-CoV-19 was administered just 63 days after the identification of the virus sequence.[5] Lipid nanoparticles (LNPs) are the premier vehicles that package, protect, and deliver mRNA inside cells, currently deployed as delivery vectors for mRNA vaccines in clinical trials.

LNPs are multicomponent lipid systems containing an ionizable lipid, a phospholipid, cholesterol, and a PEG-lipid.[6] The ionizable lipid complexes the mRNA to form a core structure while helper lipids (phospholipid and cholesterol) envelop the lipid−mRNA complex, and the PEG-lipid protects the nanoparticle shell.[7] However, the role of cholesterol in the LNP structure and the contribution of the said structure to cellular uptake and endosomal escape have yet to be revealed. LNP morphology is an essential determinant for efficient packaging and release of its cargo and remains an intriguing area of research.

The formation and structure of LNPs have been mainly studied in the context of the delivery of smaller siRNA (<30 nucleotides). However, the question remains whether or not the lessons learned from the improvements of the LNP structure for siRNA delivery apply to the mRNA due to its larger size (10^3 nucleotides).[1] Evidence suggests that the incorporation of mRNA can rearrange the LNP organization, causing the formation of inverted-hexagonal nanostructures,[8] unlike siRNA that is confined in lamellar nanostructures by ionizable lipids.[9] This is further complicated by the multi-dimensional nature of both LNP lipid formulations and the RNA nucleotide composition.

Recently, we investigated the substitution of cholesterol in LNP formulations with naturally occurring analogs with different chemical structures and the consequent effect on LNP size, mRNA encapsulation, internalization, and transfection.[10] The substitution of cholesterol (Chol) with β-sitosterol (Sito) in the formulation showed a substantial improvement in cell transfection. Upon further inspection of Sito LNPs with a cryo-transmission electron microscope (cryo-TEM), we found that Sito LNPs have a faceted surface, as opposed to spherical Chol LNPs with smooth curvature, likely due to phase separation of comprising lipids,[11] and potentially, the formation of two-dimensional lipid crystals in the LNP membrane.[8]

In this study, we investigated the structure of LNPs containing naturally occurring phytosterols (namely, β-sitosterol (Sito), fucosterol (Fuco), campesterol (Camp), and
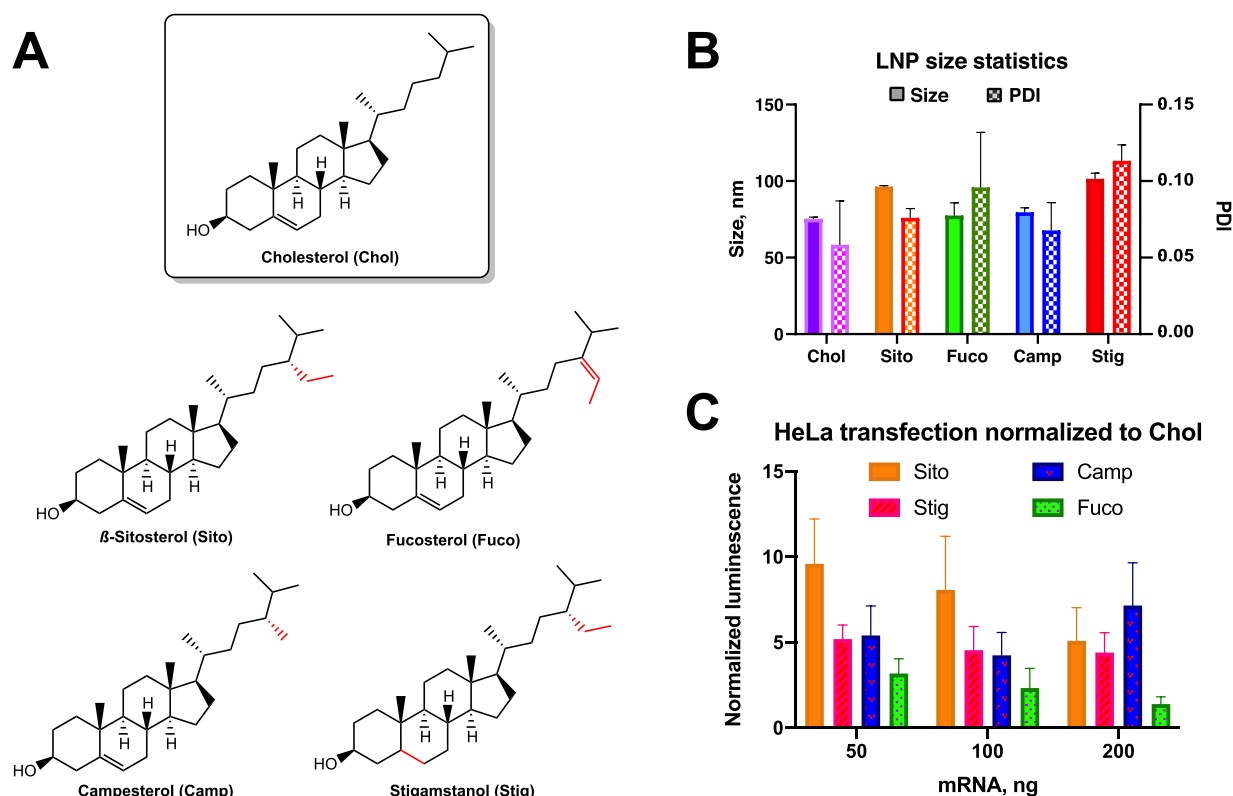
Figure 1. (A) Structures of phytosterols, or naturally occurring cholesterol analogs, used in this work. The differences from the cholesterol chemical structure are highlighted in red. (B) Hydrodynamic size and PDI of LNPs as determined by DLS ($n = 6$). (C) Transfection efficiency at 24 h in HeLa cells, normalized by Chol LNP efficiency ($n = 3$).

stigmastanol (Stig)) using cryo-TEM, thermal analysis, and a fluorescent assay (TMA-DPH probe). We found that the incorporation of Chol analogs significantly affects the morphology of the LNPs and enhances nucleic acid delivery. The findings of this study provide unique insights into the LNP structure that perhaps causes improvement in mRNA transfection. The deconvolution of the LNP structure can lead to new designs that enable efficient gene transfer.

■ RESULTS AND DISCUSSION

Basic Nanoparticle Properties. LNPs containing cholesterol analogs , DLin-MC3-DMA, DSPC, DMG-PEG-2000 (38.5:50:10:1.5 lipid molar ratios, respectively), and FLuc mRNA, were prepared using a standard microfluidic mixing procedure.[10,12] The structures of cholesterol analogs are shown in Figure 1A. Overall, all LNPs showed a narrow size distribution (see Figure 1B) as measured by dynamic light scattering (DLS) and >90% encapsulation efficiency (Figure S1). Chol LNPs had the highest mRNA encapsulation efficiency and smallest size and polydispersity index (PDI), while Stig LNPs had the largest size with the largest PDI and slightly less efficient encapsulation. Transfection of HeLa cells with prepared LNPs (Figure 1C) showed up to 10-fold improvement in gene transfection (Figure S2). At the highest dose, a slight decrease in protein expression is often observed due to the saturation of cellular machinery.[10,13−15]

Cryo-Electron Microscopy. We employed cryo-TEM to investigate the structure of LNPs (Figure 2). We found that Sito and Stig LNPs have a faceted surface, as opposed to spherical Chol and Camp LNPs. Camp, Stig, and Sito LNPs formed multilamellar structures, while Chol and Fuco LNPs

mostly formed a single bilayer. Fuco LNPs have distinctly different morphology from other LNPs, containing domains with distinctly different electron density forming at the LNP boundaries, which may be the result of lipid crystallization and mRNA separating from the lipid core.

We quantified the number of particles containing bi- and multilamellar structures and internal defects (areas of different electron densities). The results are shown in Figure 3A,B. Yanez Arteta et al. have previously proposed a lamellar structure of DLin-MC3-DMA/DSPC/DMG-PEG-2000/Chol LNPs (similar to this work) with human erythropoietin mRNA on the basis of scattering length density measurements.[8] In their work, it is suggested that the core mostly contains cationic lipid, mRNA, and cholesterol and is surrounded by layers of DSPC and PEG-lipid. The differences in particle morphology are likely due to the separation of the comprising lipids.[11] The comparison of LNP sizes measured by DLS and cryo-TEM (Figure 3C) revealed a consistently smaller size in the micrographs, likely due to the contrast challenges associated with cryo-EM where the PEG chains may not be visible. Additionally, the average thickness of the bilayers in these LNPs varies from ca. 3 nm for Chol LNPs to ca. 5 nm for Fuco LNPs, which attests to the changes in lipid organization.

These findings paint an interesting picture of particle morphology and its potential impact on gene transfection. Sito, Camp, and Stig LNPs all have a large fraction of multilamellar particles in the population (ca. 45%, 50%, and 75%, respectively); however, Camp and Stig LNPs show a similar improvement in transfection (ca. 5-fold) while improvement for Sito LNPs is ca. 10-fold. We speculate that there is an optimal percentage of multilamellar structures per
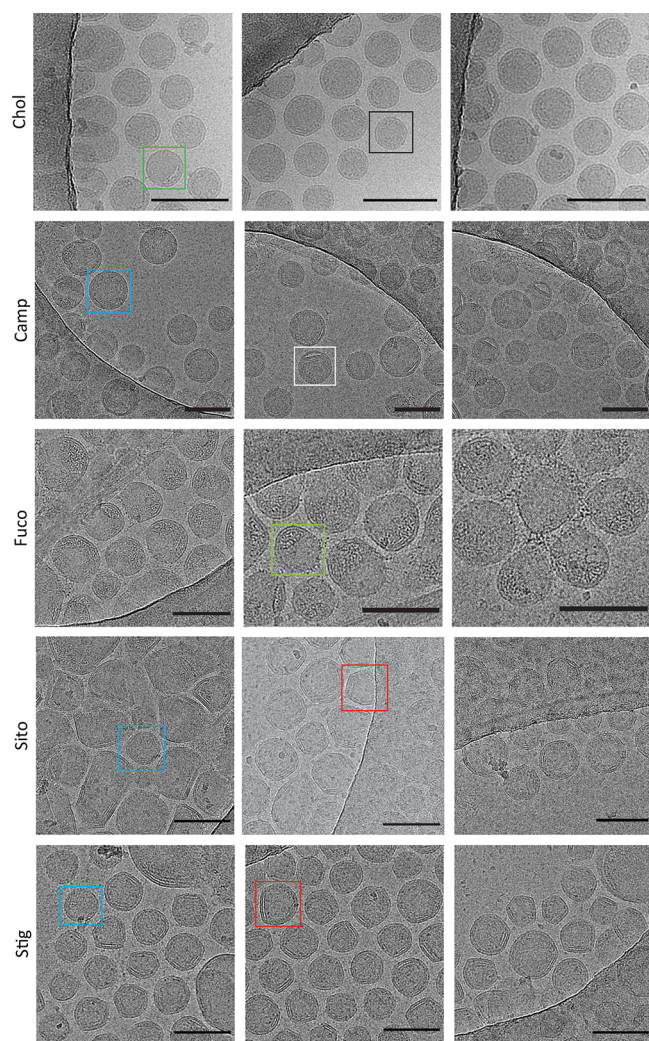
Figure 2. cryo-TEM micrographs of the phytosterol LNPs. Chol LNPs possess a dense inner core, bilamellar structure, and smooth particle curvature. Camp, Stig, and Sito LNPs all form multilamellar structures, although only Stig and Sito LNPs demonstrate a polymorphic shape, with multilamellar structures forming along the flatter edges. Fuco LNPs show inner areas with distinctly different electron density, also referred to as internal defects. Examples of LNP classification are highlighted in the boxes: green, bilamellar, internal defects; black, bilamellar, no internal defects; blue, multilamellar, no internal defects; white, multilamellar, internal defects; red, multilamellar, no internal defects, faceted. The scale bar in all images denotes 100 nm.

Figure 3. Analysis of phytosterol LNP populations as determined by cryo-TEM. (A, B) Qualitative analysis of particle morphology; (C) comparison of sizes determined by DLS ($n = 3$) and cryo-TEM ($n > 85$ for each sample).

particle population. Out of these three analogs, Camp LNPs have the highest percentage of internal defects (15%), while Sito and Stig LNPs have <2% of particles with irregularities in the internal structure. Interestingly, Sito and Stig LNPs formed faceted structures, suggesting the formation of two-dimensional crystals.[8] Camp LNPs, however, show a predominantly smooth curvature (much like the previously proposed "onion" structure).[16] Chol LNPs have a small fraction of particles with internal defects (8%) but hardly any multilamellarity. Fuco LNPs have ca. a 2-fold improved transfection compared to Chol LNPs, and 95% of Fuco LNPs have internal defects and no multilamellarity. Except for Fuco LNPs, all LNPs demonstrated a homogeneous core.

On the basis of the cryo-EM results, we can divide the phytosterol LNPs into three classes: (1) high lamellarity and
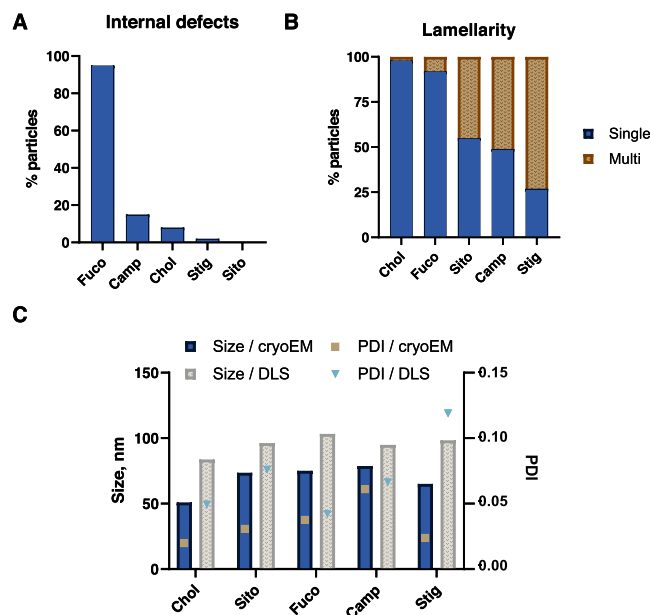
few internal defects (Sito, Camp, and Stig); (2) low lamellarity and a high number of defects (Fuco); (3) low lamellarity and few defects (Chol). We have previously shown that a polymorphic shape can influence intracellular delivery.[10] Increased lamellarity may allow multiple fusion events with the endosomal membrane. Taken together, the impact of the structure on the mechanism of gene delivery for individual analogs requires further investigation.

In the context of chemical structures of these phytosterols, all of the analogs have at least one additional carbon atom in the C24 aliphatic chain compared to cholesterol, which likely disrupts lipid packing. The structural differences align with the proposed cryo-EM classification: Sito, Camp, and Stig have saturated aliphatic tails with 1−2 additional carbon atoms compared to Chol. In comparison, Fuco has two additional carbon atoms and a double bond. It must be noted that Stig, unlike other analogs, also has a fully saturated stanol core. Iwahashi et al. previously reported that cholestanol has a lower enthalpy of fusion compared to cholesterol, confirming that the double bond in the sterol core reduces the bond strain compared to the stanol core and improves the lipid packing.[17] In conclusion, we can posit that both the sterol core and the additional substituents in the C24 alkyl tail improve transfection.

Lipid Membrane Rigidity. TMA-DPH is a fluorescent probe used to investigate lipid membrane rigidity.[18−20] As the probe lodges in the outer leaflet of the bilayer, it may take a preferential orientation and, therefore, change its spatial anisotropy (lower anisotropy = less organized bilayer structure). Bernsdorff and Winter previously used TMA-DPH in structurally similar DPPC vesicles to investigate their phase transitions and were able to identify changes in the probe orientation as a function of vesicle composition and temperature.[18] We utilized this probe to investigate if lipid membranes of phytosterol LNPs exhibit differences in rigidity, as this observation could provide more insights into their cellular uptake and endosomal escape; Sun et al. have
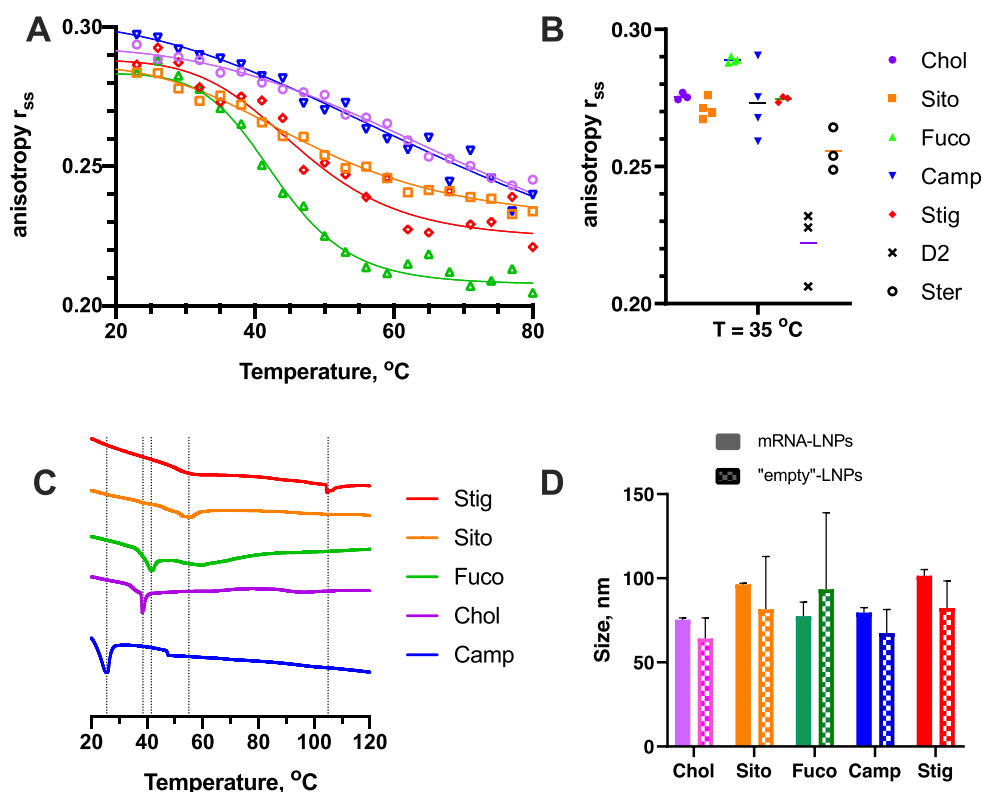
Figure 4. TMA-DPH assay and differential scanning calorimetry (DSC) data. (A) Fluorescence anisotropy of all phytosterol LNPs ($n = 4$). Error bars omitted for clarity; the lines serve as the guide to the eye. More details available in Figure S3. (B) Values of fluorescence anisotropy at 35 °C. (C) DSC curves for the freeze-dried, empty phytosterol LNPs ($n = 2$). (D) Comparison of DLS data for LNP with and without mRNA payload (PDI data available in Figure S4).

previously reported that "rigid" polymeric nanoparticles were more successful at passing the cellular barrier compared to the "soft" ones, suggesting that the higher rigidity should correlate with the higher transfection.[21] We tested the probe anisotropy in the range of 20 to 80 °C, focusing on the physiologically relevant temperatures. In addition to the cholesterol analogs mentioned above, we also tested LNPs prepared with vitamin D2 (D2) and stigmasterol (Ster) as controls, as these previously showed high mRNA encapsulation but no transfection and poor encapsulation but improved transfection compared to Chol LNPs, respectively.[10] The results are shown in Figure 4A,B.

Chol and Camp LNPs demonstrated the highest anisotropy throughout the entire tested range, followed by Sito and Stig and, last, Fuco LNPs. As mentioned before, this indicates that Fuco LNPs have the most disorganized bilayer structure. The anisotropy pattern matched for cooling and heating cycles, suggesting that the lipids do not separate during the heating process. The drop in the anisotropy with increasing temperature was expected due to the increased Brownian motion (Figure S3). Chol and Camp LNPs, as well as Sito and Stig LNPs, showed nearly identical anisotropy trends over the entire tested temperature range.

At the physiologically relevant temperature (35 °C), the TMA-DPH assay revealed marginal differences in anisotropy of analog LNPs, except for Fuco LNPs that showed higher anisotropy (ca. 0.29 vs 0.27 on average for the other phytosterol LNPs). Ster and D2 LNPs, previously identified

outliers, showed significantly lower anisotropy at 35 °C (approximately 0.25 and 0.22, respectively). These findings suggest that there is likely a Goldilocks membrane rigidity range; the somewhat fluid lipid membrane of D2 LNPs may disintegrate before the LNPs pass the cellular barrier, while the excessively rigid membrane of Fuco LNPs perhaps fails to successfully release the cargo due to their excessive stability in the biological environment. However, low encapsulation efficiency may compromise cellular uptake despite optimal rigidity. Ster LNPs demonstrated an anisotropy value more similar to the LNP baseline and were more successful at transfection than Chol LNPs; however, their encapsulation efficiency was significantly lower, likely due to the lack of free rotation of the alkyl tail.[22]

Thermal Analysis. Differential scanning calorimetry (DSC) is a thermal analysis method used to characterize phase transitions, frequently used for liposomes.[23] Phospholipid-based liposomes containing Chol analogs undergo phase transitions in the physiological temperature range,[24−26] which change lipid organization and may even induce changes in lipid membrane curvature.[27,28] These properties may have implications on the nucleic acid cargo delivery; for example, complexes of cationic liposomes containing DNA show various transfection efficiencies, depending on the organization.[29] Coupled with the membrane rigidity assay, DSC could be a useful tool in understanding the effect of Chol analogs on membrane structure[23] and, potentially, deducing whether the phase transitions of LNPs occur at the membrane surface or in
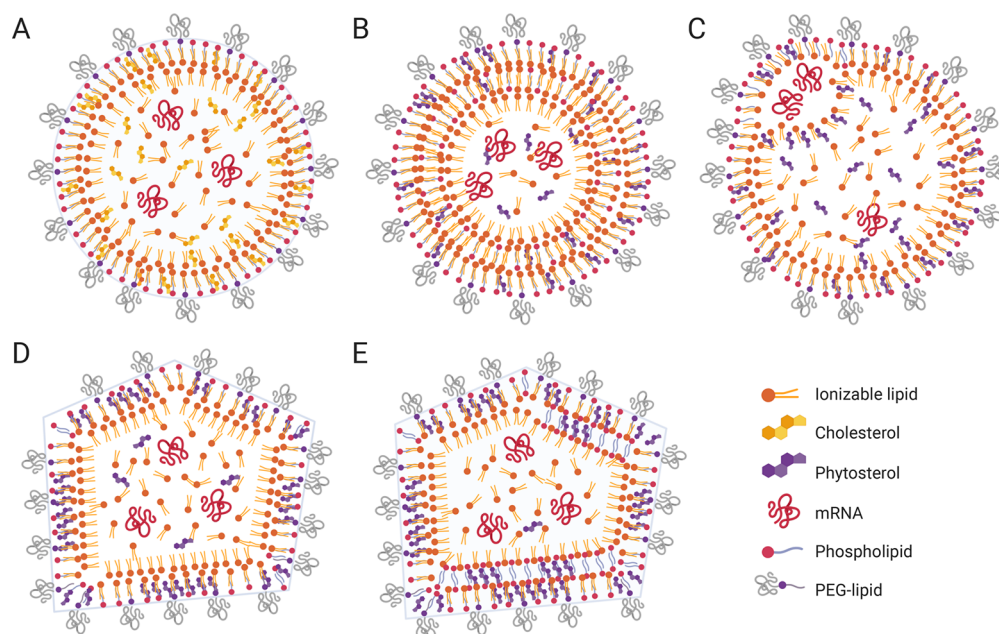
Figure 5. Hypothetical structures of LNPs identified in this work: (A) unilamellar (contains only one bilayer) perimeter, smooth particle curvature, and homogeneous core (e.g., Chol LNPs); (B) "onion" or multilamellar perimeter and homogeneous core (e.g., Camp LNPs); (C) bilamellar perimeter but lipid phase separation creates pockets, possibly containing mRNA (e.g., Fuco LNPs); (D) polymorphic or faceted (e.g., Sito and Stig LNPs); (E) polymorphic and multilamellar (e.g., Sito and Stig LNPs). The lipid ratio illustrated is not representative of that in the formulations; water omitted for clarity.

the bulk of the lipid material. Therefore, we decided to investigate the thermotropic behavior of LNPs containing no mRNA and compare the LNP thermal behavior to the results of the membrane rigidity assay. The results are shown in Figure 4C.

All tested LNPs showed distinct sharp phase transition peaks. Stig LNPs showed the highest phase transition temperature at 105 °C, while Sito, Fuco, Chol, and Camp LNPs only had one phase transition at ca. 55, 42, 38, and 26 °C, respectively. Camp and Chol LNPs also exhibit glass transitions at ca. 46 and 95 °C (respectively), while Stig and Fuco LNPs have additional broad transitions at ca. 56 and 60 °C (respectively). All of the transitions were endothermic, suggesting that these transitions correspond to melting and, thus, decreasing organization. Jovanović et al. previously reported that DPPC/Chol and Sito liposomes undergo phase transitions in a similar range, although melting temperatures depended on the lipid content.[23] These phase transitions were attributed to the gel-to-liquid transition, and it has been demonstrated that the increasing fraction of phytosterols in the liposomal formulations induces ordering in the lipid membrane, suppressing the said transition.[18,23] siRNA-LNP formulations with Chol-based cationic lipids undergo endothermic phase transitions in a similar range, which were identified as lamellar-to-inverted-hexagonal based on small-angle X-ray scattering.[30] We have previously identified that the Chol and Sito LNPs containing mRNA possess a lamellar internal structure at 25 °C,[10] which may suggest that LNPs with phytosterols undergo lamellar-to-inverted hexagonal transition when heated.

Cholesterol is known to induce membrane "stiffening" when mixed with phospholipids, increasing the membrane fluidity below and decreasing the fluidity above the gel-to-liquid transition temperature as confirmed by both DSC and the TMA-DPH assay for DPPC/Chol vesicles.[18,31] The shifting of the transition peaks should be interpreted as a measure of intermolecular interactions in LNP formulation. Reduced transition temperatures would suggest reduced intermolecular interactions.[31]

Analysis of the transition peaks among the "empty" phytosterol LNPs suggests that the Camp LNPs have weaker intermolecular interactions compared to Chol LNPs, while the rest of the LNPs have increasingly stronger intermolecular interactions. This could be interpreted as the increasing LNP membrane rigidity; therefore, Camp LNPs are the least rigid, while Stig LNPs are the most rigid. Since membrane rigidity may concur with the multilamellarity, DSC data explains why Sito and Stig LNPs both have a high degree of lamellarity and transition peaks at ca. 55 °C. Stig LNPs, however, exhibit an additional, more pronounced peak at 102 °C, which signifies the inherently different lipid arrangement in the formulation. Similarly, Fuco, Camp, and Chol LNPs show additional thermal events after the main transition; Fuco LNPs showed an additional phase transition while Chol and Camp LNPs showed glass transitions. The differences in thermotropic behavior correlate with the classification suggested on the basis of the results of cryo-EM and suggest that phytosterol LNPs may exhibit different lipid phases at physiological temperatures.

Even though empty Camp LNPs exhibit a transition at a temperature below physiological and thus could form an inverted-hexagonal phase at the temperatures above 25 °C, loading of mRNA, the addition of solvent into the LNPs, and the presence of solvent may significantly affect the lipid interactions and organization as a result. This is evident from the DLS data shown in Figure 4D. DLS analysis revealed that LNPs containing no mRNA payload possess a smaller size with a much larger deviation compared to those with mRNA, reiterating that the presence of mRNA is instrumental in the lipid self-assembly and may influence lipid phase behavior.

This assumption is further supported by TMA-DPH assay results ([Figure S3](#)), which showed no defined phase transitions between 20 and 80 °C. This observation might be the result of compromised binding of the hydrophilic TMA-DPH probe to the outer membrane layer due to the PEG shield or water displacement, previously observed in response to the incorporation of cholesterol into phospholipid membranes.[32,33] Although the previous cryo-TEM study indicates that the incorporation of siRNA into LNP formulations does not alter the LNP morphology,[9] future studies are needed to deconvolute further the effect of the solvent and the chemistry of RNA cargo as well as the lipid composition and ratios.

■ CONCLUSION

LNPs have become the gold standard in the nonviral delivery of genes. However, the LNP morphology and its effect on gene delivery remain to be uncovered. Studies with the replacement of phospholipid, PEG-lipid, and ionizable lipids have led to the deconvolution of the size, shape, and internal structure of these clinically approved materials.[34−36] Using the C24 alkyl derivatives of cholesterol, we expand on the understanding of features within the LNP structure.

The incorporation of phytosterols in place of cholesterol has a significant impact on the LNP morphology and the consequential gene transfection *in vitro*. Overall, the LNPs containing phytosterols show different degrees of rigidity and, likely, crystallinity, which explains the differences in their lamellarity, lipid partitioning, and thermal response. We summarize their hypothetical structures in [Figure 5](#).

Sito LNPs, the best performer in the *in vitro* studies, showed one broad transition peak in DSC, a high degree of lamellarity, and no internal defects; Chol LNPs, the baseline, showed a phase and a glass transition while revealing hardly any structural features. The incorporation of Stig resulted in the largest fraction of multilamellar structures and a distinctive phase transition pattern. Camp LNPs showed a thermal pattern similar to Chol yet possessed a much larger degree of multilamellarity and, potentially, the inverted-hexagonal phase at a physiological temperature. Fuco, the only phytosterol in the series containing a double bond in the alkyl chain, likely induces an entirely different lipid ordering due to the lipid separation, as evident from both the distinct fraction of internal defects and the thermal pattern. Despite the subtle variations in the chemical structures of these phytosterols, they greatly affect the lipid packing in LNP formulations. Overall, we can propose that an increase in multilamellarity and polymorphic shape results in higher gene transfection, although future studies are needed to identify the lipid phases and their effect on gene delivery.

Uncovering structural modifications that occur in an *in vivo* environment is critical to developing highly efficient systems.[37] Moreover, the delivery of RNA-based medicines to nonhepatic targets may require adjustments to the LNP structure. A case in point is the mRNA delivery to the eye, where the LNP must pass the vitreous cavity and penetrate the retinal tissue, or to the lungs, where the LNP must be nebulized to spread throughout the lung and cross the thick mucus, which are the future directions of our work. The understanding of LNP morphology and lipid composition has crucial ramifications in the prevention and treatment of infectious diseases via LNP-mRNA vaccines, such as those currently in the vanguard to tackle the unraveling of the COVID-19 pandemic.

■ ASSOCIATED CONTENT

Ⓢ Supporting Information

The Supporting Information is available free of charge at https://pubs.acs.org/doi/10.1021/acs.nanolett.0c01386.

Materials and methods, encapsulation efficiency, transfection, and full TMA-DPH assay data, DLS data for particles with and without mRNA payload, and author contributions ([PDF](#))

■ AUTHOR INFORMATION

Corresponding Author

Gaurav Sahay — *Department of Pharmaceutical Sciences, College of Pharmacy, Oregon State University, Portland, Oregon 97201, United States; Department of Biomedical Engineering, Oregon Health & Science University, Portland, Oregon 97201, United States;* ⓘ orcid.org/0000-0003-1071-0500; Phone: (503) 346-4698; Email: sahay@ohsu.edu

Authors

Yulia Eygeris — *Department of Pharmaceutical Sciences, College of Pharmacy, Oregon State University, Portland, Oregon 97201, United States*

Siddharth Patel — *Department of Pharmaceutical Sciences, College of Pharmacy, Oregon State University, Portland, Oregon 97201, United States*

Antony Jozic — *Department of Pharmaceutical Sciences, College of Pharmacy, Oregon State University, Portland, Oregon 97201, United States*

Complete contact information is available at:
https://pubs.acs.org/10.1021/acs.nanolett.0c01386

Notes

The authors declare no competing financial interest.

■ REFERENCES

(1) Sahin, U.; Karikó, K.; Türeci, Ö. MRNA-based therapeutics-developing a new class of drugs. *Nat. Rev. Drug Discovery* **2014**, *13*, 759−780.

(2) Kowalski, P. S.; Rudra, A.; Miao, L.; Anderson, D. G. Delivering the Messenger: Advances in Technologies for Therapeutic mRNA Delivery. *Mol. Ther.* **2019**, *27*, 710−728.

(3) Miller, J. B.; Zhang, S.; Kos, P.; Xiong, H.; Zhou, K.; Perelman, S. S.; Zhu, H.; Siegwart, D. J. Non-Viral CRISPR/Cas Gene Editing In Vitro and In Vivo Enabled by Synthetic Nanoparticle Co-Delivery of Cas9 mRNA and sgRNA. *Angew. Chem., Int. Ed.* **2017**, *56*, 1059−1063.

(4) Zhang, X.; Li, B.; Luo, X.; Zhao, W.; Jiang, J.; Zhang, C.; Gao, M.; Chen, X.; Dong, Y. Biodegradable Amino-Ester Nanomaterials for Cas9 mRNA Delivery in Vitro and in Vivo. *ACS Appl. Mater. Interfaces* **2017**, *9*, 25481−25487.

(5) Moderna. *Moderna's Work on a Potential Vaccine Against COVID-19*; Moderna, Inc.; https://www.modernatx.com/modernas-work-potential-vaccine-against-covid-19, accessed on 2020-03-17.

(6) Rizk, M.; Tuzmen, S. Update on the clinical utility of an RNA interference-based treatment: focus on Patisiran. *Pharmacogenomics Pers. Med.* **2017**, *10*, 267−278.

(7) Cullis, P. R.; Hope, M. J. Lipid Nanoparticle Systems for Enabling Gene Therapies. *Mol. Ther.* **2017**, *25*, 1467−1475.

(8) Yanez Arteta, M.; Kjellman, T.; Bartesaghi, S.; Wallin, S.; Wu, X.; Kvist, A. J.; Dabkowska, A.; Székely, N.; Radulescu, A.; Bergenholtz, J.; Lindfors, L. Successful reprogramming of cellular protein production through mRNA delivered by functionalized lipid nano-particles. *Proc. Natl. Acad. Sci. U. S. A.* **2018**, *115*, E3351−E3360.

(9) Kulkarni, J. A.; Darjuan, M. M.; Mercer, J. E.; Chen, S.; Van Der Meel, R.; Thewalt, J. L.; Tam, Y. Y. C.; Cullis, P. R. On the Formation and Morphology of Lipid Nanoparticles Containing Ionizable Cationic Lipids and siRNA. *ACS Nano* **2018**, *12*, 4787−4795.

(10) Patel, S.; Ashwanikumar, N.; Robinson, E.; Xia, Y.; Mihai, C.; Griffith, J. P.; Hou, S.; Esposito, A. A.; Ketova, T.; Welsher, K.; Joyal, J. L.; Almarsson, Ö.; Sahay, G. Naturally-occurring cholesterol analogues in lipid nanoparticles induce polymorphic shape and enhance intracellular delivery of mRNA. *Nat. Commun.* **2020**, *11*, 983.

(11) Imam, Z. I.; Kenyon, L. E.; Ashby, G.; Nagib, F.; Mendicino, M.; Zhao, C.; Gadok, A. K.; Stachowiak, J. C. Phase-Separated Liposomes Enhance the Efficiency of Macromolecular Delivery to the Cellular Cytoplasm. *Cell. Mol. Bioeng.* **2017**, *10*, 387−403.

(12) Leung, A. K.; Tam, Y. Y. C.; Chen, S.; Hafez, I. M.; Cullis, P. R. Microfluidic Mixing: A General Method for Encapsulating Macro-molecules in Lipid Nanoparticle Systems. *J. Phys. Chem. B* **2015**, *119*, 8698−8706.

(13) Patel, S.; Ashwanikumar, N.; Robinson, E.; Duross, A.; Sun, C.; Murphy-Benenato, K. E.; Mihai, C.; Almarsson, Ö.; Sahay, G. Boosting Intracellular Delivery of Lipid Nanoparticle-Encapsulated mRNA. *Nano Lett.* **2017**, *17*, 5711−5718.

(14) Coats, M. T.; Bydlinski, N.; Maresch, D.; Diendorfer, A.; Klanert, G.; Borth, N. mRNA Transfection into CHO-Cells Reveals Production Bottlenecks. *Biotechnol. J.* **2020**, *15*, 1900198.

(15) Kulkarni, J. A.; Myhre, J. L.; Chen, S.; Tam, Y. Y. C.; Danescu, A.; Richman, J. M.; Cullis, P. R. Design of lipid nanoparticles for in vitro and in vivo delivery of plasmid DNA. *Nanomedicine* **2017**, *13*, 1377−1387.

(16) Viger-Gravel, J.; Schantz, A.; Pinon, A. C.; Rossini, A. J.; Schantz, S.; Emsley, L. Structure of Lipid Nanoparticles Containing siRNA or mRNA by Dynamic Nuclear Polarization-Enhanced NMR Spectroscopy. *J. Phys. Chem. B* **2018**, *122*, 2073−2081.

(17) Iwahashi, M.; Minami, H.; Suzuki, T.; Koyanagi, M.; Yao, H.; Ema, K.; Ashizawa, K. Thermodynamic Properties of Steroids: 5-cholesten-3-beta-ol, 5-alpha-cholestan-3-beta-ol, and 5-beta-cholestan-3-alpha-ol. *J. Oleo Sci.* **2001**, *50*, 693−699.

(18) Bernsdorff, C.; Winter, R. Differential Properties of the Sterols Cholesterol, Ergosterol, β-Sitosterol, trans-7-Dehydrocholesterol, Stigmasterol and Lanosterol on DPPC Bilayer Order. *J. Phys. Chem. B* **2003**, *107*, 10658−10664.

(19) Illinger, D.; Duportail, G.; Mely, Y.; Poirel-Morales, N.; Gerard, D.; Kuhry, J. G. A comparison of the fluorescence properties of TMA-DPH as a probe for plasma membrane and for endocytic membrane. *Biochim. Biophys. Acta, Biomembr.* **1995**, *1239*, 58−66.

(20) Valeur, B. *Encyclopedia of Applied Physics*; Major Reference Works; Wiley-VCH Verlag GmbH & Co. KGaA: Weinheim, Germany, 2009; pp 477−531.

(21) Sun, J.; Zhang, L.; Wang, J.; Feng, Q.; Liu, D.; Yin, Q.; Xu, D.; Wei, Y.; Ding, B.; Shi, X.; Jiang, X. Tunable rigidity of (polymeric core)-(lipid shell) nanoparticles for regulated cellular uptake. *Adv. Mater.* **2015**, *27*, 1402−1407.

(22) Lopez, S.; Bermudez, B.; Montserrat-De La Paz, S.; Jaramillo, S.; Varela, L. M.; Ortega-Gomez, A.; Abia, R.; Muriana, F. J. Membrane composition and dynamics: A target of bioactive virgin olive oil constituents. *Biochim. Biophys. Acta, Biomembr.* **2014**, *1838*, 1638−1656.

(23) Jovanović, A. A.; Balanč, B. D.; Ota, A.; Ahlin Grabnar, P.; Djordjević, V. B.; Šavikin, K. P.; Bugarski, B. M.; Nedović, V. A.; Poklar Ulrih, N. Comparative Effects of Cholesterol and β-Sitosterol on the Liposome Membrane Characteristics. *Eur. J. Lipid Sci. Technol.* **2018**, *120*, 1800039.

(24) Winter, R.; Czeslik, C. Pressure effects on the structure of lyotropic lipid mesophases and model biomembrane systems. *Z. Kristallogr. - Cryst. Mater.* **2000**, *215*, 454−474.

(25) Tenchov, B. On the reversibility of the phase transitions in lipid-water systems. *Chem. Phys. Lipids* **1991**, *57*, 165−177.

(26) Krivanek, R.; Okoro, L.; Winter, R. Effect of Cholesterol and Ergosterol on the Compressibility and Volume Fluctuations of Phospholipid-Sterol Bilayers in the Critical Point Region: A Molecular Acoustic and Calorimetric Study. *Biophys. J.* **2008**, *94*, 3538−3548.

(27) Gruner, S. M. Intrinsic curvature hypothesis for biomembrane lipid composition: a role for nonbilayer lipids. *Proc. Natl. Acad. Sci. U. S. A.* **1985**, *82*, 3665−3669.

(28) Brown, M. F. Curvature forces in membrane lipid-protein interactions. *Biochemistry* **2012**, *51*, 9782−95.

(29) Rädler, J. O.; Koltover, I.; Salditt, T.; Safinya, C. R. Structure of DNA-cationic liposome complexes: DNA intercalation in multi-lamellar membranes in distinct interhelical packing regimes. *Science (Washington, DC, U. S.)* **1997**, *275*, 810−814.

(30) Zhang, J.; Fan, H.; Levorse, D. A.; Crocker, L. S. Interaction of cholesterol-conjugated ionizable amino lipids with biomembranes: Lipid polymorphism, structure-activity relationship, and implications for siRNA delivery. *Langmuir* **2011**, *27*, 9473−9483.

(31) McElhaney, R. N. The use of differential scanning calorimetry and differential thermal analysis in studies of model and biological membranes. *Chem. Phys. Lipids* **1982**, *30*, 229−259.

(32) Haque, E.; McIntosh, T. J.; Lentz, B. R. Influence of lipid composition on physical properties and PEG-mediated fusion of curved and uncurved model membrane vesicles: "Nature's own" fusogenic lipid bilayer. *Biochemistry* **2001**, *40*, 4340−4348.

(33) Simon, S. A.; Mcintosh, T. J.; Latorre, R. Influence of cholesterol on water penetration into bilayers. *Science (Washington, DC, U. S.)* **1982**, *216*, 65−67.

(34) Kulkarni, J. A.; Witzigmann, D.; Leung, J.; Tam, Y. Y. C.; Cullis, P. R. On the role of helper lipids in lipid nanoparticle formulations of siRNA. *Nanoscale* **2019**, *11*, 21733−21739.

(35) Kim, H.; Leal, C. Cuboplexes: Topologically Active siRNA Delivery. *ACS Nano* **2015**, *9*, 10214−10226.

(36) Rietwyk, S.; Peer, D. Next-Generation Lipids in RNA Interference Therapeutics. *ACS Nano* **2017**, *11*, 7572−7586.

(37) Paunovska, K.; Sago, C. D.; Monaco, C. M.; Hudson, W. H.; Castro, M. G.; Rudoltz, T. G.; Kalathoor, S.; Vanover, D. A.; Santangelo, P. J.; Ahmed, R.; Bryksin, A. V.; Dahlman, J. E. A Direct Comparison of in Vitro and in Vivo Nucleic Acid Delivery Mediated by Hundreds of Nanoparticles Reveals a Weak Correlation. *Nano Lett.* **2018**, *18*, 2148−2157.